Chiral Cooperativity and Solvent-Induced Tautomerism Effects in Electronic Circular Dichroism Spectra of [2.2]Paracyclophane Ketimines

Ingolf Warnke,[†] Sefer Ay,[‡] Stefan Bräse,*[,‡] and Filipp Furche*[,†]

Department of Chemistry, University of California, Irvine, 1102 Natural Sciences II, Irvine, California 92697-2025, and Institut für Organische Chemie, Universität Karlsruhe (TH), Fritz-Haber-Weg 6, 76131 Karlsruhe, Germany

Received: March 21, 2009; Revised Manuscript Received: May 5, 2009

[2.2]Paracyclophanes with chiral ketimine side chains constitute a class of highly versatile and enantioselective ligands for catalytic carbon−carbon bond forming reactions. Proper matching of the side chain and [2.2]paracyclophane configurations induces chiral cooperativity, which is key to high selectivities. Here we show that the absolute configuration of both chirotropic elements may be fully resolved by CD spectroscopy and time-dependent density functional calculations. Different ketimine side chain conformations of the diastereomers perturb the planar chiral [2.2]paracyclophane chromophore. This leads to characteristic changes in the measured CD spectra and the specific rotation allowing for the simultaneous assignment of the absolute configuration of both chiral elements. Our results give rise to a simple rule relating sign and magnitude of the specific rotation and the first band of the CD spectra to the absolute configuration of both chiral elements. We infer a tautomeric equilibrium between an *ortho*-hydroquinone-imine and an *ortho*-quinone-enamine from strong solvatochromism observed in the CD spectra.

1. Introduction

The synthesis of enantiomerically pure compounds is a major challenge in contemporary organic chemistry.[1−8] Building on the achievements of Knowles,[9] Kagan,[10] Noyori,[11] and many others, today's organic chemists are able to realize many transformations in a stereocontrolled and enantioselective manner using metal catalysis.[12] These transformations crucially depend on the efficiency, selectivity, and availability of catalysts based on enantiomerically pure ligands.[13] While classical ligands mostly exhibit central chirality, planar chirality has played a pivotal role for many modern ligand systems, such as ferrocenyl ligands.[14,15] Recently, planar chiral *ortho*-hydroxy [2.2]paracyclophane ketimine ligands were introduced to asymmetric catalysis (Figures 1 and 2).[16] By now, these ligands have become a powerful and versatile tool for asymmetric C−C bond formation:[17,18] [2.2]Paracyclophane ketimines **1** afford 1,2-addition[16] and conjugate 1,4-addition[19] of organozinc compounds to aldehydes and ketones as well as dialkyzinc addition to imines[20] in a highly asymmetric and efficient manner; see Figure 3.

Chiral cooperativity between the planar chiral [2.2]paracyclophane unit and the asymmetric α carbon atom in the ketimine side chain is crucial for high yields and selectivities.[20] Thus, knowledge of the absolute configuration of both chirotropic elements is vital for synthetic applications. Determination of the absolute configuration of [2.2]paracyclophane ketimines is challenging: (i) two or more chiral elements are present; (ii) fully stereoselective synthesis is rarely possible; (iii) X-ray analysis is expensive and time-consuming, may be impaired by twinning, and requires growth of crystals. Some ligands remain in an oily state and do not crystallize at all.

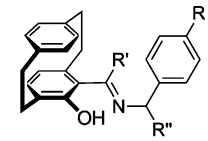

1

Figure 1. [2.2]Paracyclophane ketimine ligands **1**.

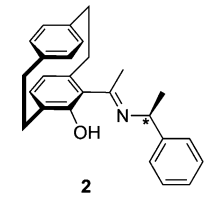

2

Figure 2. [2.2]Paracyclophane ketimine derivative **2** exhibiting planar and central chirality.

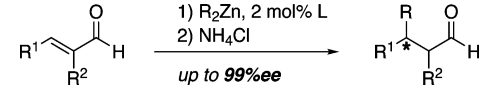

Figure 3. Conjugate 1,4-addition reaction catalyzed by the ligand-organozinc complex.

Here we determine the absolute configuration of [2.2]paracyclophane ketimine ligands from measurements of the electronic circular dichroism (CD), optical rotation (OR),[21,22] and time-dependent density functional calculations.[23] Since their introduction in 2000,[24] the combination of CD spectroscopy and time-dependent density functional calculations has widely been used to determine the absolute configuration of *isolated* chirality elements exhibiting central,[25] axial,[26] planar[27] and topological[24] chirality. The application of time-dependent density functional theory (TDDFT) to systems containing multiple interacting chiral elements such as **2** represents a new level of difficulty and is much less established.[21] Since the CD and OR of [2.2]paracyclophane ketimines in the near UV are largely

* Corresponding authors. E-mail: S.B., stefan.braese@ioc.uka.de; F.F., filipp.furche@uci.edu.
[†] University of California, Irvine.
[‡] Universität Karlsruhe (TH).

10.1021/jp902563z CCC: $40.75
Published on Web 05/28/2009

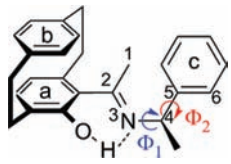

Figure 4. Definition of $\Phi_1 = \angle(2,3,4,5)$ and $\Phi_2 = \angle(3,4,5,6)$ in compound **2**. C(4) is the asymmetric carbon atom. The aromatic rings are denoted **a**, **b**, and **c**.

determined by the [2.2]paracyclophane chromophore, diastereomers may be distinguished due to the interaction of the former with the chiral (1-phenyl)-ethyl side chain. This interaction is mainly electrostatic in nature and results from different conformations of the diastereomers. We condense our results into a simple rule relating CD and OR measurements directly to the absolute configuration of both chirality elements of the ligand. In contrast to X-ray analysis, our method is inexpensive and fast, allowing for the parallel determination of the absolute configuration of whole sample arrays. This is a crucial prerequisite for combinatorial catalyst optimization.[28,29]

A striking feature of the CD spectra of compound **2** is a strong solvent dependence of the low-energy bands. We show that this solvatochromism is likely due to solvent-induced tautomerism between an *ortho*-hydroquinone-imine and an *ortho*-quinone-enamine form of **2**. Recently, the low-barrier tautomerism occurring in related salicylidene anilines has attracted attention[30−33] because of its potential use in photo- and thermochromic materials.[34] To the best of our knowledge, solvent-dependent tautomerism of [2.2]paracyclophane ketimines has not been observed before. We speculate that the position of the tautomeric equilibrium has consequences for the catalyst's stereoselectivity.

2. Experimental Details

The diastereomers of compound **2** were synthesized over five steps using the methods of ref 35. In previous studies,[16,36] we used X-ray analysis to correlate the absolute configuration of ligand **2** to the absolute configuration of the product of a catalytic reaction. All CD measurements were performed using a JASCO J-815-150S CD spectrometer. Solutions (6.7×10^{-4} M) of the ligands were prepared and transferred in a 1 mm thick quartz cell. All CD spectra were measured at 293 K. Commercially available solvents were employed and freshly distilled before use. The optical rotations were measured in solution using a Perkin-Elmer 241 polarimeter (Na-D-line, 589 nm) in a tempered glass cell of 10 cm length at 293 K.

3. Computational Details

All structure optimizations were performed using the meta-generalized gradient approximation functional of Tao, Perdew, Staroverov, and Scuseria (TPSS, ref 37) and fine (size m4, ref 38) numerical integration grids. Karlsruhe split valence plus polarization (SVP, ref 39) basis sets were utilized unless otherwise stated. The continuum solvent model COSMO[40] was used to account for solvent effects in structure optimizations and calculations of the CD spectra of (R_p,*X*)-**2**, ($X = R, S$). Computed structures were validated by comparison to X-ray and correlated wave function results[41] for [2.2]paracyclophane; see the Supporting Information for further details. The barrier for the rotation of the (1-phenyl)ethyl side chain of the hydroquinone-imine tautomer of (R_p,*R*)-**2** was investigated by varying the dihedral angle Φ_1 defined in Figure 4 in steps of 5° and optimizing all other internal degrees of freedom at the TPSS level in the gas phase. Subsequently, the barrier height was computed in gas phase single point calculations using the hybrid density functional of Perdew, Burke, and Enzerhof (PBE0).[42] In the same manner, the minimum energy path for the hydroquinone-imine−quinone-ketimine tautomerization of (R_p,*R*)-**2a** was determined by varying the OH bond length in steps of 2.6 pm. All CD spectra were computed using TDDFT response theory[43,44] and the PBE0 hybrid functional. CD spectra were simulated by Gaussian broadening and superposition of the computed rotatory strengths R_{0n} of the transitions. The following empirical line widths were used: 0.15 eV (toluene) and 0.30 eV (chloroform). For comparison with experimental CD spectra, the intensities of the theoretical spectra were scaled by a factor of 0.5. While absolute intensities are commonly reproduced within a factor of 2 within TDDFT calculations,[45] trends in relative CD intensities are often much more accurate. We assign configurations by comparing *ratios* of CD intensities, which do not depend on scaling factors. Optical rotations were computed within TDDFT response theory[46] using the PBE0 hybrid functional and diffuse augmented[47−49] SVP basis sets and COSMO. All computations were carried out using the TURBOMOLE program suite.[50]

4. Results

4.1. Conformational Analysis. In all compounds considered here, the two aromatic units of the paracyclophane moiety are conformationally rigid. Furthermore, the OH−N hydrogen bridge keeps the (1-phenyl)ethyl side chain in-plane with its adjacent phenyl ring. Thus, the two dihedral angles Φ_1 and Φ_2, defined in Figure 4, are the only relevant conformational degrees of freedom.

For each diastereomer, structure optimization yielded two conformations of different energy, denoted (R_p,*X*)-**2a** and (R_p,*X*)-**2b**, where $X = R, S$; see Figure 5. Rotamers (R_p,*X*)-**2a** and (R_p,*X*)-**2b**, which differ by their Φ_1 value, are separated by a barrier of 7.9 kcal/mol. Φ_2 was found to adjust to a given Φ_1 value, and there are no rotamers differing in Φ_2 only. (R_p,*R*)-**2a** is 3.4 kcal/mol lower in energy than (R_p,*R*)-**2b**. The situation is reversed for the (R_p,*S*) diastereomer, where (R_p,*S*)-**2b** is 4.7 kcal/mol lower in energy than (R_p,*S*)-**2a**. Hence, stable diastereomers differ by the relative orientation of the [2.2]paracyclophane subsystem and the phenyl group **c** of the (1-phenyl)ethyl side chain. As discussed in the next section, this has important implications for the chiroptical properties at room temperature.

4.2. Computed CD Spectra. As shown in Figure 6, the computed CD spectra of compound **2** exhibit two characteristic bands in the 300−400 nm region denoted A and B. The intensity and shape of bands A and B are determined by the four lowest singlet excited states listed in Table 1. All low-energy excitations are essentially localized in the planar chiral [2.2]paracyclophane moiety, as expected. The first excitation at 356 nm is well separated and due to a transition between the two frontier orbitals shown in Figure 7. The highest occupied molecular orbital (HOMO) may be viewed as a π orbital of the aromatic subsystem **a** (see Figure 4), whereas the lowest unoccupied molecular orbital (LUMO) resembles the π^* orbital of the C=N double bond.

Since the CD spectrum of **2** is dominated by bands of the [2.2]paracyclophane chromophore, the sign of the first band at 355 nm is an indicator of the absolute configuration of the [2.2]paracyclophane unit: the R_p configuration results in a positive sign of the first band (see Figure 8), while the S_p configuration results in a negative sign. It is more difficult to distinguish diastereomers that differ only in the side chain configuration using CD. As shown in Figure 8, the CD spectra

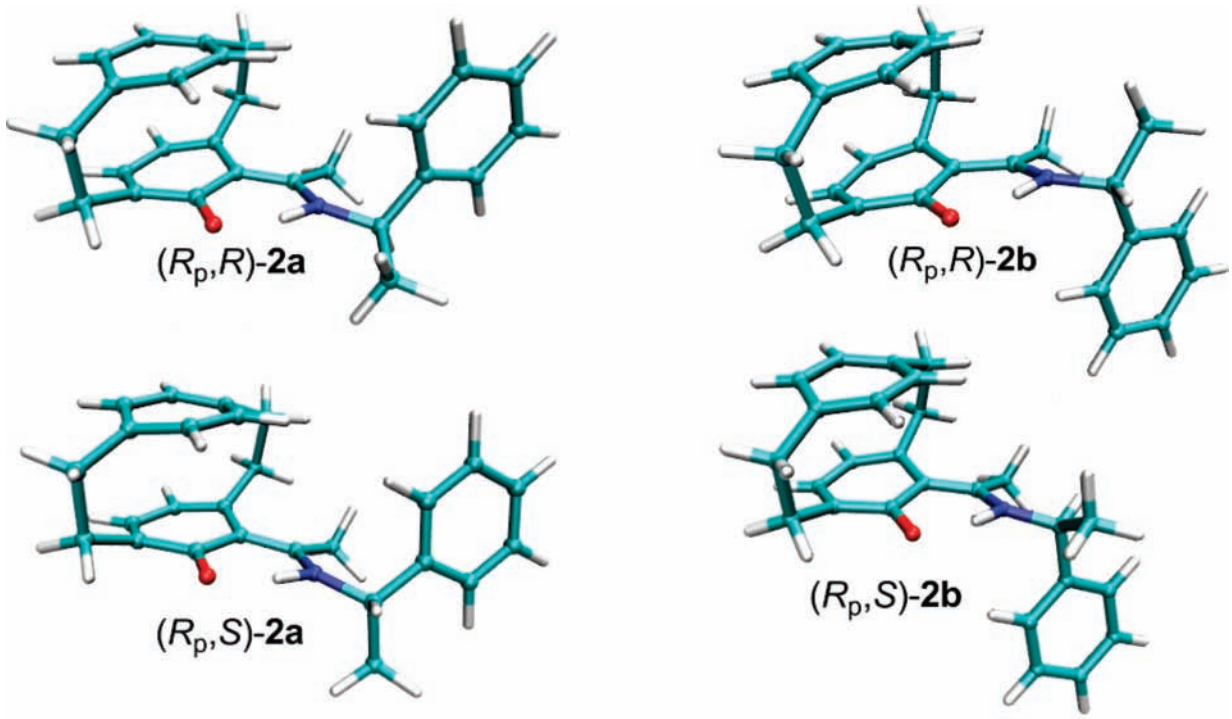

Figure 5. Structures of the low-energy and high-energy conformers of the (R_p,R) (upper panel) and (R_p,S) diastereomer (lower panel) of compound **2**. (R_p,R)-**2a** and (R_p,S)-**2b** are energetically favored.

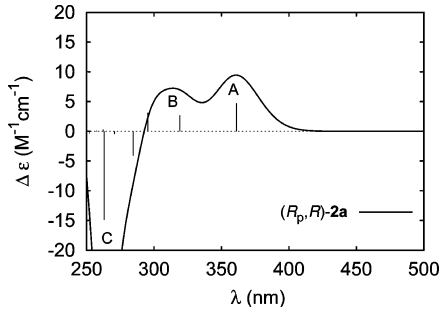

Figure 6. Computed CD of (R_p,R)-**2a**. See Table 1 for an assignment.

TABLE 1: Energy ΔE (in nm), Rotatory Strength R (in 10^{-40} cgs) and the Dominant Orbital Contributions of the Four Lowest Excitations of the (R_p,R) Low-Energy Diastereomer (R_p,R)-2a[a]

State	ΔE	Band	R	Orbitals	Assignment
2 ^{1}A	361	A	47.2	99a→100a, 96%	π (**a**) → π^* (−C=N)
3 ^{1}A	319	B	27.0	98a→100a, 94%	π (**b**) → π^* (−C=N)
4 ^{1}A	295	B	31.4	97a→100a, 90% 98a→100a, 3%	π (**b**) → π^* (−C=N)
5 ^{1}A	285		−41.2	94a→100a, 51% 95a→100a, 30% 93a→100a, 12%	N-lone pair and π (**c**) → π^* (−C=N)

[a] The excitations contribute to the bands A and B of the CD spectrum (see Figure 6). A qualitative assignment is given in the last column. The aromatic rings **a**, **b**, and **c** are defined in Figure 4.

of the (R_p,R) and (R_p,S) diastereomers in the *same configuration* are indeed approximately identical. However, there is a sizable difference between the spectra of *different* conformers. Since the energetic ordering of the two conformers is interchanged in (R_p,R) and (R_p,S), the intensity difference of the A band may be used to determine the side chain configuration.

What causes the different A band intensities that make the diastereomers distinguishable? A simple rationale is based on a change in orientation between the electric transition dipole moment vector $\boldsymbol{\mu}_{0n}$ and the magnetic transition dipole moment vector $\mathbf{m}_{0n}$: The rotatory strength of a transition from the electronic ground state to the nth excited singlet state is[51]

$$R_{0n} = \mathrm{Im}(\boldsymbol{\mu}_{0n} \cdot \mathbf{m}_{0n}) = |\boldsymbol{\mu}_{0n}||\mathbf{m}_{0n}|\cos\theta \qquad (1)$$

θ is the angle enclosed by $\boldsymbol{\mu}_{0n}$ and $\mathbf{m}_{0n}$. Thus, a parallel orientation of the two vectors (θ close to 0°) results in high CD intensity, whereas a nearly perpendicular orientation (θ close to 90°) results in low CD intensity. For the transitions studied here, the magnitudes of the transition moment vectors hardly change with θ; thus, the change in the rotatory strengths R_{0n} may be attributed to a change in θ.

Table 2 summarizes the computed θ and R_{01} values in both conformations of the (R_p,R) and (R_p,S) diastereomers. The (R_p,R)-**2a** low-energy conformer has $\theta = 81°$, leading to low CD intensity of the A band. In the corresponding high-energy conformer (R_p,R)-**2b**, $\theta = 66°$ leads to high CD intensity of the A band. The situation is reversed for the (R_p,S) conformers: Here, the high-energy conformer (R_p,S)-**2a** has $\theta = 75°$, the low-energy conformer (R_p,S)-**2b** has $\theta = 65°$. Thus, the (R_p,S)-**2a** high-energy conformer has a less intense first CD band compared to the low-energy conformer (R_p,S)-**2b**. Since the difference in θ is smaller compared to the (R_p,R) diastereomer, the difference in the CD intensity of the first band is less pronounced. The relative orientation θ of the transition dipole moments $\boldsymbol{\mu}_{0n}$ and $\mathbf{m}_{0n}$ establishes a link between the conformation and the intensity of band A in the CD spectrum. Importantly, the configuration of the (1-phenyl)ethyl side chain affects the intensity of the first CD band only indirectly via the preferred conformation.

The absolute configuration of **2** may also be inferred from measurements of the OR. The computed specific rotations

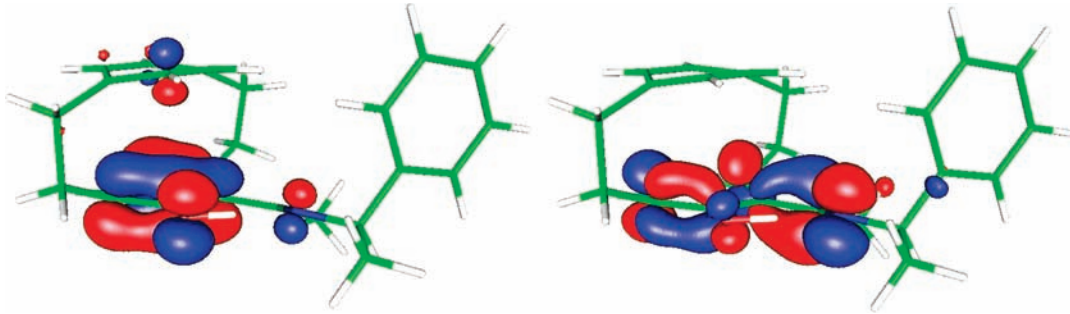

Figure 7. HOMO (left) and LUMO (right) of the low-energy conformer of **2**. The HOMO (molecular orbital 99) can be viewed as a π orbital of ring **a** (see Figure 4). The LUMO (molecular orbital 100) has considerable C=N π^* character.

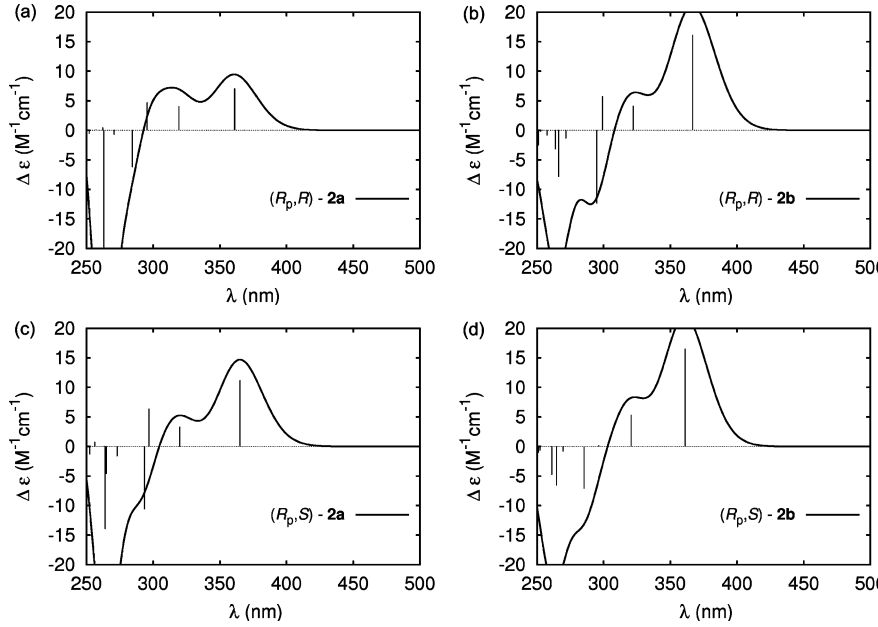

Figure 8. Computed CD spectra of both conformers of the (R_p,R)-**2** (upper panel) and (R_p,S)-**2** diastereomers (lower panel). (R_p,R)-**2a** and (R_p,S)-**2b** are energetically favored.

TABLE 2: Computed Rotatory Strengths R_{01} (10^{-40} cgs) and Angles θ (deg) between the Electric Transition Dipole Moments μ_{01} and the Magnetic Transition Dipole Moments m_{01} for the High-Energy and Low-Energy Conformation of the (R_p,R) and (R_p,S) Diastereomers of Compound 2[a]

configuration	conformation	Φ_1	θ	R_{01}	[α]
(R_p,R)	**a** (low energy)	89	81	46.8	180
(R_p,R)	**b** (high energy)	−66	66	98.6	1059
(R_p,S)	**b** (low energy)	−87	65	105.0	1240
(R_p,S)	**a** (high energy)	53	75	68.4	546

[a] Φ_1 (deg) is the dihedral angle defined in Figure 4. Specific rotations [α] (deg·(dm(g/cm^3))$^{-1}$) are computed for λ = 589 nm and include solvent effects (toluene).

of the diastereomers are displayed in Table 2. A positive sign of the OR corresponds to a positive sign of the lowest CD band and vice versa. Moreover, a large absolute value of the OR corresponds to a high CD intensity and a small magnitude of the OR leads to a weak CD band. Our findings reflect that, in the long-wavelength limit, the OR of compound **2** is dominated by the rotatory strength R_{01} of the lowest allowed transition. This is in qualitative agreement with a sum-over-states analysis of the optical rotation,[52] and the OR−structure relationship of compound **2** may be understood in terms of its CD. However, these findings are not easily generalized to other systems. The convergence of the sum-over-states expression for the OR is well-known to be system-dependent.[53]

4.3. Assignment of the Absolute Configuration. The theoretical and experimental CD spectra of compound **2** are compared in Figure 9. Since the sign of the A band determines the configuration of the planar chiral [2.2]paracyclophane subunit, spectrum 9-**a** corresponds to S_p and spectrum 9-**b** to R_p configuration. The side chain configuration is determined by means of the A band intensities, as discussed in section 4.2. The ratio of the A band intensities of the experimental spectra shown in Figure 9 is 0.61. The theoretical value of 0.69 is in good agreement with the experimental value. Thus, we may assign the side chain configuration of the ligands corresponding to both spectra in Figure 9 to be R. This assignment is supported by a comparison of the measured and computed specific optical rotations. The experimental values are 692 and 242 deg·(dm(g/cm^3))$^{-1}$ for the (S_p,R) and the (R_p,R) diastereomers, respectively, and in qualitative agreement with the computed values, which are 1240 deg·(dm(g/cm^3))$^{-1}$ for the (S_p,R) and 180 deg·(dm(g/cm^3))$^{-1}$ for the (R_p,R) diastereomer; compare Table 2. Since the computed CD spectra of (R_p,S) and (R_p,R) enantiomers are mirror images of the (S_p,R) and (S_p,S) spectra, the identification of the latter is straightforward.

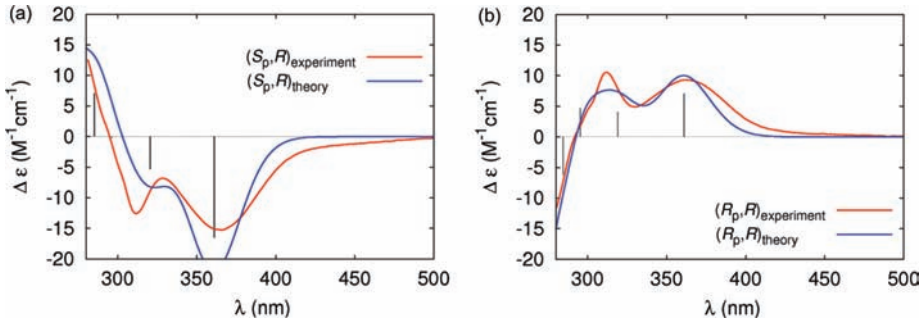

Figure 9. Experimental CD of a pair of diastereomers recorded in toluene is compared to corresponding theoretical data. The predicted difference in the absolute intensities of band A (see Figure 6) spectra is present in the measured spectra.

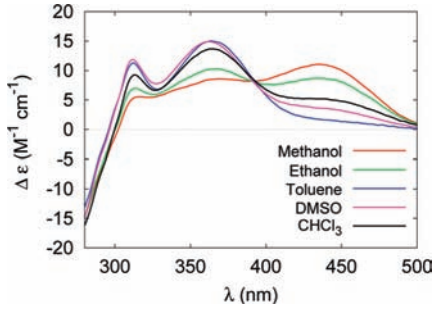

Figure 10. Experimental CD spectra of the (R_p,*S*) diastereomer recorded in solvents of different polarity.

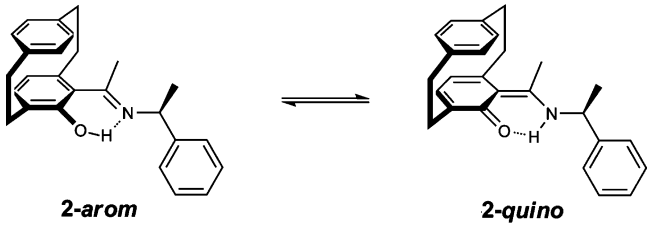

Figure 11. Tautomerism of compound **2**. **2-arom** is the *ortho*-hydroquinone-imine form and **2-quino** is the *ortho*-quinone-enamine form of **2**.

5. Solvatochromism

As shown in Figure 10, compound **2** exhibits unusually strong solvatochromism of the CD spectra indicating significant solvent-induced structural changes. The presence of an isosbestic point[54] in the experimental solvent series suggests an equilibrium of two spectroscopically distinct species.

The calculations predict two tautomers **2-arom** and **2-quino**, presented in Figure 11. In the gas phase, (R_p,*S*)-**2-arom** is computed to be 0.86 kcal/mol lower in energy than (R_p,*S*)-**2-quino** (PBE0/SVP). The shift of the hydrogen position and other significant structural changes (see Supporting Information) suggest that **2-arom** is an *ortho*-hydroquinone-imine tautomer with more aromatic character and that **2-quino** is an *ortho*-quinone-enamine tautomer. This is also supported by the difference in the computed HOMO−LUMO gaps (PBE0/SVP) between the aromatic and the quinoidal tautomer amounting to 4.29 and 3.27 eV, respectively. The computed dipole moment of **2-arom** is 2.9 D; the *ortho*-quinoidal tautomer **2-quino** has a computed dipole moment of 4.1 D. The computed CD spectra of structures **2-arom** and **2-quino** are compared in Figure 12. The CD spectrum of the hydroquinone-imine form has already been discussed in section 4.2. Detailed information about the low-energy transitions of the orthoquinone-enamine tautomer is provided in the Supporting Information. In both tautomers, the lowest transitions are dominated by HOMO−LUMO

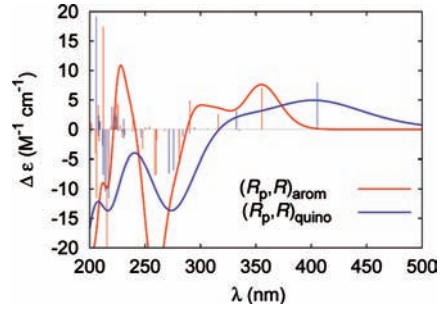

Figure 12. Computed CD spectra of the *ortho*-quinone-enamine and the *ortho*-hydroquinone-imine tautomer of the (R_p,*R*) diastereomer.

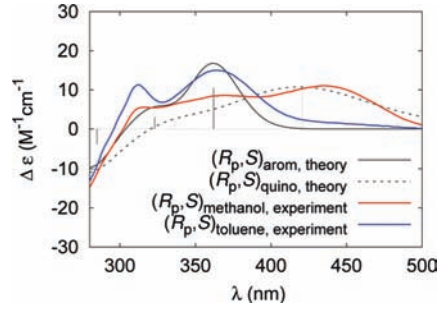

Figure 13. Computed and measured CD of the tautomers (R_p,*S*)-**2-arom** and (R_p,*S*)-**2-quino**. The less polar solvent favors the less polar *ortho*-hydroquinone-imine form whereas the more polar solvent promotes the *ortho*-quinone-enamine form of **2**.

contributions. The large 50 nm red shift of the first transition in the orthoquinoidal tautomer reflects the difference in the HOMO−LUMO gap of 0.57 eV.

Figure 13 compares the computed CD spectra of the two tautomers with experimental spectra recorded in toluene and methanol. Toluene (dielectric constant $\varepsilon = 2.4$) is the least polar solvent considered in our experimental section, and methanol ($\varepsilon = 33$) is the most polar solvent. The computed spectrum of the less polar tautomer **2-arom** compares well with the spectrum recorded in toluene, while the computed spectrum of the more polar tautomer **2-quino** is in good agreement with the spectrum recorded in methanol.

We performed calculations including solvation effects within the COSMO continuous solvation model to study solvent effects on the tautomeric equilibrium. The computed energy difference between **2-arom** and **2-quino** was found to depend on the solvent polarity. **2-quino** is favored in polar media, while **2-arom** is preferred in unpolar media, as expected from the computed dipole moments of 4.1 and 2.9 D. Experimental CD spectra in solvents of intermediate polarity are well reproduced by a Boltzmann weighted superposition of the computed spectra of both tautomers, as shown in Figure 14. Within the rigid-

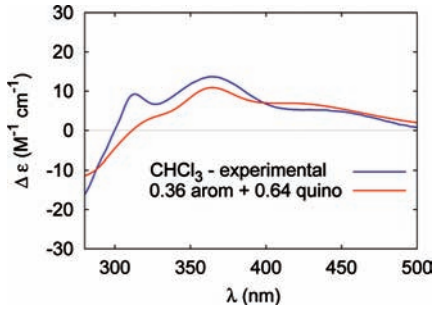

Figure 14. Boltzmann-weighted superposition of *ortho*-quinone-enamine and *ortho*-hydroquinone-imine CD spectra versus CD spectrum of (R_p,*S*)-**2** recorded in chloroform.

rotator-harmonic-oscillator approximation, the entropy difference between the tautomers is negligible at room temperature and the Boltzmann factors may be determined from the electronic energies. Disagreement between theory and experiment is found for the highly polar solvent dimethyl sulfoxide (DMSO) (ε = 47.2); see Figure 10: The experimental spectrum is not in line with the expectation that increasing solvent polarity shifts the equilibrium position toward the (more polar) *ortho*-quinone-ketimine tautomer. Possible reasons include specific interactions between DMSO and the solute, although explorative calculations showed a high energetic penalty (ca. 25 kJ/mol) for solvent-induced break-up of the intramolecular hydrogen bond.

The computed potential energy barrier for proton transfer is 1.7 kcal/mol in vacuo. This low value agrees with the experimental observation that the two tautomers coexist in solution. Filarowski and co-workers find a decrease of the proton transfer barrier in hydrogen-bonded substituted salicylidene aniline derivatives[30,31] with increasing steric crowding close to the hydrogen bond. The small barrier we report for the [2.2]paracyclophane ketimine **2a** is in qualitative agreement with this observation. Harada and co-workers investigate the solid state thermochromism in salicylidene anilines.[32] According to their results changes in the fluorescence spectra are due to a temperature-induced shift of the tautomeric equilibrium. This provides further evidence for the unusual solvent-induced tautomerism in [2.2]paracyclophane ketimines reported here.

6. Conclusions

The theoretically obtained relation between the angle θ and the molecular structure suggests the following simple rule to determine the absolute configuration of [2.2]paracyclophanes **1** from their chiroptical properties.

Chiral Cooperativity Rule (CCR):

(i) If the sign of the A band or OR is positive (negative), the paracyclophane moiety has R_p (S_p) configuration.

(ii) The absolute intensity of band A or the absolute OR value is lower in the (R_p,*R*) diastereomer and its enantiomer and higher in the (R_p,*S*) diastereomer and its enantiomer.

(ii) results from an asymmetric perturbation of the inherently chiral [2.2]paracyclophane chromophore. This perturbation is probably a predominantly electrostatic effect caused by different conformations of the chiral (1-phenyl)ethyl side chain: The different electrostatic environment changes the orientation of the 2 ^{1}A transition dipole moments, which strongly affects the rotatory strength. (ii) holds if the energy difference between the **a** and **b** conformers is sufficiently large, i.e., if R′ and R″ are such that respective diastereomers correspond to different rotamers. The CCR provides a first guess at the absolute configuration of [2.2]paracyclophane ketimines. While we expect it to be of considerable practical value, we recommend checking it whenever possible, e.g., by TDDFT calculations. Table 3 displays the OR of some experimentally studied ligands[16] whose absolute configurations were established by X-ray analysis. The phenyl group on the chiral carbon atom is crucial for (ii) to hold. (ii) may break down if the phenyl group is replaced by other groups, e.g., by a cyclohexyl group in a system with R′ = $-C_3H_7$ and R″ = $-CH_3$. In this case, (i) still holds and the planar chirality determines the sign of the OR, but the absolute value of the OR is now approximately the same for both diastereomers.

TABLE 3: Measured OR of Some Experimentally Relevant Systems[16]

configuration					
X-ray	CCR	R	R′	R″	$[\alpha]^{589}$
(R_p,*S*)	(R_p,*S*)	−H	−Me	−Et	1108
(S_p,*S*)	(S_p,*S*)	−H	−Me	−Et	−357
(R_p,*S*)	(R_p,*S*)	−F	−Me	−Me	733
(S_p,*S*)	(S_p,*S*)	−F	−Me	−Me	−241
(R_p,*S*)	(R_p,*S*)	−OMe	−Me	−Me	918
(S_p,*S*)	(S_p,*S*)	−OMe	−Me	−Me	−187
(R_p,*S*)	(R_p,*S*)	−H	−*p*-Br-C_6H_4	−Me	790
(S_p,*S*)	(S_p,*S*)	−H	−*p*-Br-C_6H_4	−Me	−396

The CD spectra of **2** were found to exhibit strong solvatochromism in the A band region. We have presented evidence that this solvatochromism is caused by a solvent-dependent equilibrium between hydroquinone-imine and quinone-enamine tautomers of **2**. Our calculations predict significant differences in the infrared spectra of the tautomers that may be used to further corroborate our hypothesis in the future (see Supporting Information). Since the first step in the catalytic cycle is believed to be a metalation of the paracyclophane ketimine, it is conceivable that the tautomeric equilibrium has an effect on the formation rate of the active complex. The relative tautomer stability is a new variable that may be exploited to study the catalytic reaction mechanism and to optimize enantioselectivity.

Acknowledgment. F.F. acknowledges support by the NSF Center for Chemical Innovation at the Space-Time Limit (CaSTL), grant no. CHE-0533162. This work was in part supported by the Centre for Functional Nanostructures (CFN) of the Deutsche Forschungsgesellschaft (DFG) within project C3.9. S.A. was supported by a Kekulé stipend of the Fonds der Chemischen Industrie.

Supporting Information Available: Computed Cartesian atomic coordinates of both tautomeric forms of the considered conformers of the (R_p,*S*) and (R_p,*R*) diastereomers, assignment of the computed CD spectra (rotatory strengths, energies and dominant orbital contributions of the 15 lowest transitions) of both tautomeric forms of the (R_p,*S*) low-energy conformer, and computed infrared spectra of both tautomeric forms of the (R_p,*R*) low-energy conformer. This material is available free of charge via the Internet at http://pubs.acs.org.

References and Notes

(1) Nicolaou, K. C.; Sorensen, E. J. *Classics in Total Synthesis*; VCH: Weinheim, 1996.
(2) Bräse, S.; Dahmen, S.; Höfener, S.; Lauterwasser, F.; Kreis, M.; Ziegert, R. *Synlett* **2004**, 2647–2669.
(3) Knowles, W. *Angew. Chem., Int. Ed.* **2002**, *41*, 1996.
(4) Knowles, W. *Angew. Chem.* **2002**, *114*, 2096.
(5) Noyori, R. *Angew. Chem., Int. Ed.* **2002**, *41*, 2008.
(6) Noyori, R. *Angew. Chem.* **2002**, *114*, 2108.
(7) Sharpless, K. *Angew. Chem., Int. Ed.* **2002**, *41*, 2024.

(8) Sharpless, K. *Angew. Chem.* **2002**, *114*, 2126.
(9) Knowles, W.; Sabacky, M. *J. Chem. Soc., Chem. Commun.* **1968**, 1445.
(10) Kagan, H.; Dang, T. *J. Am. Chem. Soc.* **1972**, *94*, 6429.
(11) Noyori, R. *Science* **1990**, *248*, 1994.
(12) Christmann, M.; Bräse, S. *Asymmetric Synthesis—The Essentials*; VCH: Weinheim, 2006.
(13) Yoon, T. P.; Jacobsen, E. N. *Science* **2003**, *299*, 1691–1693.
(14) Arrayás, R. G.; Adria, J.; Carretero, J. C. *Angew. Chem., Int. Ed.* **2006**, *45*, 7674–7715.
(15) Dai, L.-X.; Tu, T.; Deng, W.-P.; Hou, X.-L. *Acc. Chem. Res.* **2003**, *36*, 659–667.
(16) Lauterwasser, F.; Nieger, M.; Mansikkamäki, H.; Nättinen, K.; Bräse, S. *Chem.—Eur. J.* **2005**, *11*, 4509–4525.
(17) Pu, L.; Ju, H.-B. *Chem. Rev.* **2001**, *101*, 757–824.
(18) Knochel, P.; Singer, R. D. *Chem. Rev.* **1993**, *93*, 2117–2188.
(19) Höfener, S.; Bräse, S. *Angew. Chem., Int. Ed.* **2005**, *44*, 7879–7881.
(20) Dahmen, S.; Bräse, S. *J. Am. Chem. Soc.* **2002**, *124*, 5940–5941.
(21) Petrovic, A.; Polavarapu, P.; Drabowicz, J.; Łyzwa, P.; Mikołajczyk, M.; Wieczorek, W.; A., B. *J. Org. Chem.* **2008**, *73*, 3120–3129.
(22) Polavarapu, P. *Int. J. Quantum Chem.* **2006**, *106*, 1809–1814.
(23) Marques, M.; Ullrich, C.; Nogueira, F.; Rubio, A.; Burke, K.; Gross, E. *Time-Dependent Density Functional Theory*; Springer Verlag, 2006.
(24) Furche, F.; Ahlrichs, R.; Wachsmann, C.; Weber, E.; Sobanski, A.; Vögtle, F.; Grimme, S. *J. Am. Chem. Soc.* **2000**, *122*, 1717–1724.
(25) Drabowicz, J.; Dudziński, B.; Mikołajczyk, M.; Wand, F.; Dehlavi, A.; Goring, J.; Park, M.; Rizzo, C.; Polavarapu, P. L.; Biscarini, P.; Wieczorec, M.; Majzner, W. *J. Org. Chem.* **2001**, *66*, 1122–1129.
(26) Mori, T.; Inoue, Y.; Grimme, S. *J. Phys. Chem. A* **2007**, *111*, 4222–4234.
(27) Mori, T.; Inoue, Y.; Grimme, S. *J. Phys. Chem. A* **2007**, *111*, 7995–8006.
(28) Ding, K.; Du, H.; Yuan, Y.; Long, J. *Chem.—Eur. J.* **2004**, *10*, 2872–2884.
(29) Reetz, M. *Angew. Chem., Int. Ed.* **2001**, *40*, 284–310.
(30) Filarowski, A.; Koll, A.; Glowiak, T. *J. Mol. Struct.* **2002**, *615*, 97–108.
(31) Filarowski, A.; Koll, A.; Glowiak, T. *J. Chem. Soc., Perkin Trans 2* **2002**, 835–842.
(32) Harada, J.; Fujiwara, T.; Ogawa, K. *J. Am. Chem. Soc.* **2007**, *129*, 16216–16221.
(33) Kluba, M.; Lipowski, P.; Filarowski, A. *Chem. Phys. Lett.* **2008**, *463*, 426–430.
(34) Hadjoudis, E. *Photochromism*; Elsevier: Amsterdam, 1990; pp 685–712.
(35) Rozenberg, V.; Danilova, T.; Sergeeva, E.; Voronstov, E.; Starikova, Z.; Lysenko, K.; Belokon, Y. *Eur. J. Org. Chem.* **2000**, *19*, 3295–3303.
(36) Lauterwasser, F.; Gall, J.; Höfener, S.; Bräse, S. *Adv. Synth. Catal.* **2006**, *348*, 2068–2074.
(37) Tao, J.; Perdew, J.; Staroverov, V. N.; Scuseria, G. E. *Phys. Rev. Lett.* **2003**, *91*, 146401.
(38) Treutler, O.; Ahlrichs, R. *J. Chem. Phys.* **1995**, *102*, 346–354.
(39) Schäfer, A.; Horn, H.; Ahlrichs, R. *J. Chem. Phys.* **1992**, *97*, 2571–2577.
(40) Klamt, A.; Schüürmann, G. *J. Chem. Soc., Perkin Trans.2* **1993**, 799–805.
(41) Grimme, S. *Chem.—Eur. J.* **2004**, *10*, 3423–3429.
(42) Perdew, J. P.; Ernzerhof, M.; Burke, K. *J. Chem. Phys.* **1996**, *105*, 9982–9985.
(43) Furche, F.; Rappoport, D. In Density functional methods for excited states: equilibrium structure and electronic spectra. In *Computational Photochemistry*; Olivucci, M., Ed.; Elsevier: Amsterdam, 2005; Vol. 16, Chapter III.
(44) Bauernschmitt, R.; Ahlrichs, R. *Chem. Phys. Lett.* **1996**, *256*, 454–464.
(45) Elliott, P.; Furche, F.; Burke, K. *Rev. Comp. Chem.* **2009**, *26*, 91–165.
(46) Grimme, S.; Furche, F.; Ahrlichs, R. *Chem. Phys. Lett.* **2002**, *361*, 321–328.
(47) Schäfer, A.; Huber, C.; Ahlrichs, R. *J. Chem. Phys.* **1994**, *100*, 5829–5835.
(48) Kendall, R. A.; Dunning, T. H., Jr.; Harrison, R. J. *J. Chem. Phys.* **1992**, *96*, 6796–6806.
(49) Dunning, T. H., Jr. *J. Chem. Phys.* **1989**, *90*, 1007–1023.
(50) Ahlrichs, R.; Bär, M.; Häser, M.; Horn, H.; Kölmel, C. *Chem. Phys. Lett.* **1989**, *162*, 165–169, see also http://www.turbomole.com.
(51) Moffitt, W.; Moscowitz, A. *J. Chem. Phys.* **1959**, *30*, 648–660.
(52) Polavarapu, P. L.; Chakraborty, D. K.; Ruud, K. *Chem. Phys. Lett.* **2000**, *319*, 595–600.
(53) Wiberg, K.; Wang, Y.; Wilson, S.; Vaccaro, P.; Cheeseman, J. *J. Phys. Chem. A* **2006**, *110*, 13995–14002.
(54) Berova, N.; Nakashini, K.; Woody, R. *Circular dichroism: principles and applications*; Wiley-VCH, New York, 2000.

JP902563Z